Modelling incident-band and infra gravity wave dynamics on rocky shore platforms

McCall, Robert T.; Masselink, G.; Austin, Martin; Poate, T.; Jager, Teun

Published: 01/06/2017

Peer reviewed version

Coastal Dynamics 2017
Paper No. 144

MODELLING INCIDENT-BAND AND INFRAGRAVITY WAVE DYNAMICS ON ROCKY SHORE PLATFORMS

Robert McCall[1], Gerd Masselink[2], Martin Austin[3], Tim Poate[4] and Teun Jager[5]

Abstract

Incident-band and infragravity wave transformation on five rocky shore platforms is simulated using a numerical model. The model is calibrated using measurements of bed roughness and hydrodynamics under mild to energetic wave conditions. Validation of the model show that the model is capable of reproducing wave heights across the platform with little scatter (scatter index 0.07 – 0.27) and bias (-0.05 – + 0.02 m). Model calibration shows a strong relation between incident-band wave-related bed friction parameter values and platform roughness, as well as between infragravity wave-related bed friction parameter values and roughness once small-scale topographic details are removed from the model bed elevation. Sensitivity studies show that on even relatively smooth platforms, bed friction may dissipate significant amounts of infragravity wave energy.

Key words: rock platforms, wave dissipation, infragravity wave, bottom roughness, numerical modelling, XBeach.

1. Introduction

Approximately three quarters of the world's coastline consists of rocky and cliffed coasts (Bird, 2000). Rocky shore platforms, low-gradient rock surfaces that occur within or close to the intertidal zone and often backed by cliffs (Trenhaile, 1987; Sunamura, 1992), play an important role on such coasts by dissipating incident-band waves and reducing the amount of incident-band wave energy reaching the shoreline (cf. Trenhaile, 1983), both through wave breaking and bottom roughness.

While dissipation of incident-band wave energy on rocky shore platforms has been known for many decades, more recent studies have investigated the dynamics of infragravity waves on rocky shore platforms (e.g., Beetham and Kench, 2011; Marshall and Stephenson, 2011; Ogawa, et al., 2011; 2015) and have found infragravity wave height to increase over the platform. Dickson, et al. (2013) suggest that infragravity waves may therefore play an important role in the erosion and geomorphic development of rocky shore platforms and may drive cliff retreat over larger distances and longer time scales than currently assumed.

Despite their potential importance in rock platform morphodynamics and cliff retreat, few studies have attempted to simulate incident-band and infragravity wave dynamics transformation on these coasts using numerical models. Because of this, there are currently few guidelines for simulating wave transformation on rocky shore platforms, in particular with regard to the prediction of wave dissipation due to bottom roughness and the transformation and dissipation of infragravity waves.

The present work aims to increase our capacity to quantitatively model incident-band and infragravity wave transformation and dissipation across rocky shore platforms through the use of the numerical model XBeach (Roelvink, et al., 2009). The model is calibrated and validated using new and unique data collected on five rocky shore platforms under energetic wave conditions (Poate, et al. 2016; submitted). Using the validated model as a numerical laboratory, this work discusses the role of bed friction on incident-band and infragravity wave transformation on rock platforms and examines methods for the estimation of model bed friction parameters from measured platform roughness.

[1]Deltares, Boussinesqweg 1, 2629HV Delft, the Netherlands. robert.mccall@deltares.nl
[2]School of Marine Science and Engineering, Plymouth University, United Kingdom, gerd.masselink@plymouth.ac.uk
[3]School of Ocean Sciences, Bangor University, Menai Bridge United Kingdom, m.austin@bangor.ac.uk
[4]School of Marine Science and Engineering, Plymouth University, United Kingdom, timothy.poate@plymouth.ac.uk
[5]Deltares, Boussinesqweg 1, 2629HV Delft, the Netherlands. Currently working at Van Oord.

2. Model description

The model used in this study is the open-source, process-based model XBeach (Roelvink, et. al., 2009). The model has previously successfully been applied to simulate storm impacts on sandy (e.g., McCall, et al., 2010; Dissanayake, et al., 2014; De Vet, et al., 2015), urbanized (Smallegan, et al., 2015) and gravel (Masselink et al., 2015; McCall, et al., 2015) coasts. Recently, the model has been used to simulate wave transformation and hydrodynamics on coral reef coasts (Van Dongeren, et al., 2012; Quataert, et al., 2015). The model has not however, been previously applied on, or validated for, rocky coasts.

The XBeach model allows a number of modes for the calculation of wave motions. In this study, the so-called surf-beat mode is used (standard mode), which resolves variations in incident-band (or, high-frequency) wave energy at the wave group time scale, but does not resolve high-frequency (HF) intra-wave motions. The wave energy balance in XBeach is given in Eq. 1 (in 1D-form):

$$\frac{\partial A}{\partial t}+\frac{\partial c_g A}{\partial x}=-\frac{D_b+D_f}{\sigma} \tag{1}$$

in which $A=E/\sigma$ is wave action, E is wave energy, σ is the radian wave frequency, t and x are the temporal and spatial coordinates, respectively, c_g is the wave group velocity, and D_b and D_f are dissipation terms related to wave breaking and bed friction, respectively.

For dissipation due to wave breaking, the breaker formulation of Roelvink (1993) is used with default, or site-specific breaker parameter γ (cf. Roelvink, et al., 2009). Wave energy due to bed friction is described by Eq. 2:

$$D_f=\frac{2}{3\pi}\rho f_w\left(\frac{\pi H_{rms}}{T_{m-1,0}\sinh(kh)}\right) \tag{2}$$

where ρ is water density, f_w is the wave friction factor, H_{rms} is the root mean square wave height, $T_{m-1,0}$ is a spectral wave period, k is the wave number based on $T_{m-1,0}$ and h is the water depth.

HF wave-averaged flow, including tides, wave set-up, wave-driven currents, and infragravity (or, LF) motions are solved in XBeach using the non-linear shallow water equations, given in Eq. 3 in their 1D-form:

$$\begin{gathered}\frac{\partial \eta}{\partial t}+\frac{\partial h u^L}{\partial x}=0\\ \frac{\partial u^L}{\partial t}+u^L\frac{\partial u^L}{\partial x}-\nu_h\frac{\partial^2 u^L}{\partial x^2}=-g\frac{\partial \eta}{\partial x}+\frac{F_x}{\rho h}-\frac{\tau_{bx}^E}{\rho h}\end{gathered} \tag{3}$$

where η is the water surface elevation, u^L is the Lagrangian depth-averaged velocity, ν_h is the horizontal viscosity coefficient, g is the gravitational constant, F_x is wave forcing due to radiation stress gradients (resulting from variations in HF wave energy) and τ_{bx}^E is the bed friction for flow, based on the Eulerian velocity:

$$\tau_{bx}^E=c_f\rho u^E\sqrt{\left(1.16u_{rms}\right)^2+\left(u^E\right)^2} \tag{4}$$

and c_f is the flow friction factor, u_{rms} is the RMS orbital velocity due to HF waves, $u^E=u^L-u^S$ is the Eulerian velocity, and u^S is the Stokes velocity, see Roelvink, et al., (2009) for further details.

3. Field data description

Unique field measurements were carried out during the winter of 2014 – 2015 at four rocky shore platform sites in the UK and one in Ireland (Poate, et al., submitted): Freshwater West (FWW; Figure 1B), Lilstock (LST; Figure 1C), Hartland Quay (HLQ; Figure 1D), Portwrinkle (PTW; Figure 1E) and Doolin (DOL, Ireland; Figure 1A), as part of the WASP (Waves Across Shore Platforms) project. The morphology of the rock platform at all sites was surveyed using a terrestrial laser scanner (Leica P20) to produce a high-resolution (0.1 m x 0.1 m grid) digital elevation model (DEM) of the platform (Poate, et al., submitted). The roughness of each platform was quantified using the high-resolution DEM and the rugosity parameter (k_R; Table 1), defined as $1\text{-}A_r/A_a$, where A_r is the spatial unit surface area and A_a is the geometric surface of the area within one spatial unit. The value of k_R becomes zero for infinitely smooth platforms ($A_r = A_a$) and unity for infinitely rough platforms ($A_r << A_a$).

Water levels were measured at all sites using a cross-shore array of 12 – 15 pressure transducers (PTs; Table 1) spanning the intertidal zone. The PTs recorded pressure at 4 Hz during 8 – 13 consecutive tides. The measured pressure time series were subsequently corrected for atmospheric pressure and dynamic pressure depth attenuation following Nielsen (1989) to generate time series of water surface elevation. At all sites, wave heights recorded at the most seaward PT varied over the consecutive tides from relatively calm (H_s 0.1 – 0.7 m) to energetic (H_s 1.6 – 2.7 m) conditions (Table 1). Further details regarding data collection at these sites can be found in Poate, et al. (2016; submitted).

Measured time series of water surface elevation at the PTs were further separated into a slowly-varying (tide, set-up and surge) component, LF wave motions and HF wave motions. To this end, the measured water surface elevation time series were discretized into 20-minute bursts. For each burst, the mean water level was used to define the tidal component, and time series of LF and HF motions derived from a Fourier transform of the residual (total minus tidal) water level time series. A split frequency of 0.033 Hz was used to distinguish between LF and HF motions at the swell dominated DOL, FWW, HLQ and PTW sites, and a split frequency of 0.055 Hz was used at LST.

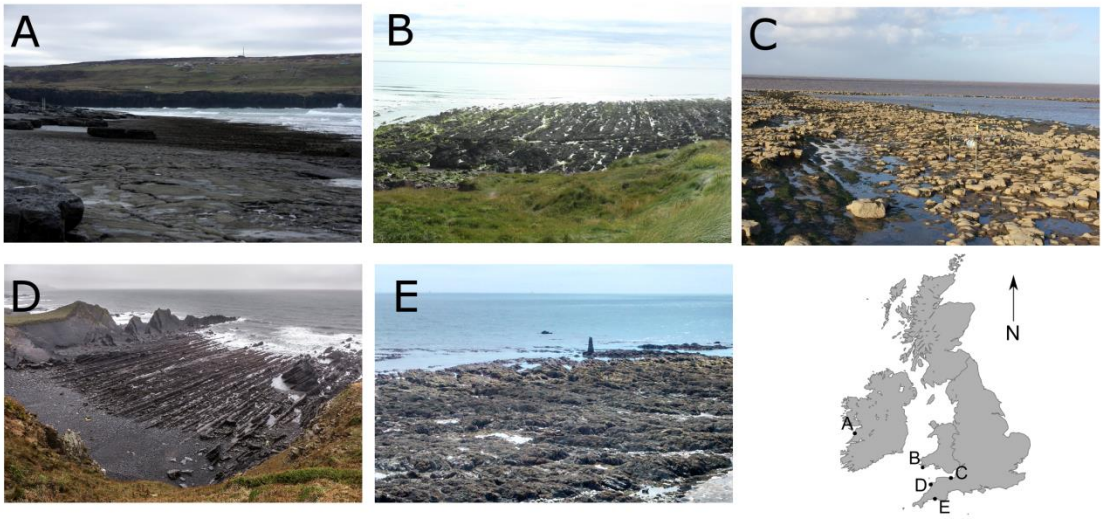

Figure 1. Overview of rocky shore platform sites: DOL (A), FWW (B); LST (C); HLQ (D); PTW (E).

Table 1. Overview of platform properties, measured hydrodynamic conditions, and data collection.

Parameter	DOL	FWW	HLQ	LST	PTW
Bedrock (-)	Limestone	Sandstone	Sandstone/ shale	Mudstone	Slate/ siltstone
Platform width (m)	160	210	140	325	180
Rugosity (k_R)	0.020	0.062	0.029	0.015	0.090
H_s (min–max) (m)	0.30–1.87	0.52–2.69	0.65–1.60	0.11–1.75	0.42–1.71
T_p (min–max) (s)	8.9–16.0	8.4–16.0	7.5–10.1	5.8–9.4	7.3–13.9
Number of tides (-)	13	8	12	8	8
Number of PTs (-)	15	14	12	15	12

4. Model setup

One-dimensional, cross-shore profile XBeach models were set up along the line of the PT arrays for each platform, extending from the seaward-most PT to a landward location of the platform (or cliff) above maximum wave run-up. The grid size was kept constant in the entire model domain, and was set at 0.5 m for all site models. The bed level in the models was kept constant (no morphological change) and was interpolated from the measurements of the bed along the main instrument line.

The XBeach models require time series of HF wave energy (for the wave action balance, Eq. 1) and tide levels and incident LF waves (for the non-linear shallow water equations, Eq. 3) as boundary conditions at the seaward edge of the model domain. Time series of HF wave energy were derived from a Hilbert-transform of the HF surface elevation signal measured at the seaward-most PT, resulting in a time-varying wave energy envelope at the seaward boundary of the model. In this analysis, all HF motions at the seaward-most PT were assumed to be entering the model (no reflected HF energy).

Time series of 20-minute average water levels measured at the seaward-most PT were used to impose tidal boundary conditions on the models. Time series of incident LF waves were derived from the measured LF water surface elevation at three seaward PTs, after removal of the outgoing wave signal using the method of Mansard and Funk (1980).

5. Model calibration

Data from two tides were used to calibrate three model parameters at each platform. The calibration of these parameters was carried out using a two-step approach, in which the first step is used to calibrate the wave-related friction factor f_w using data from outside the surf zone, and the second step is used to calibrate the wave breaker parameter γ using data from inside the surf zone and the flow-related (LF wave-related) friction factor c_f using data from inside and outside the surf zone. In both cases, the edge of the surf zone was defined as the most seaward PT where $\max\left(H_{s,i}, H_{s,i+1}\right)/\min\left(h_{i\to i+1}\right) \geq \gamma_b$, where $H_{s,i}$ and $H_{s,i+1}$ are the measured significant wave height at the PT and its seaward neighbour, respectively, $\min\left(h_{i\to i+1}\right)$ is the minimum water depth between the PT and its seaward neighbour, and γ_b is the Miche criterion.

Model skill in reproducing HF and LF wave heights during the model calibration is quantified in a unified skill parameter S that describes model error and correlation with respect to the measurements (higher is better):

$$S(x) = \frac{1}{2}\left(1 - SI(x) + \rho(x)\right) \tag{5}$$

in which ρ is the Pearson correlation coefficient:

$$\rho(x) = \frac{\mathrm{cov}\left(x_{\mathrm{modelled}}, x_{\mathrm{measured}}\right)}{\sigma_{x_{\mathrm{modelled}}}\sigma_{x_{\mathrm{measured}}}} \tag{6}$$

and *SI* is the scatter index, or normalized root-mean-square error:

$$\mathrm{SI}(x) = \frac{E_{rms}(x)}{\max\left(\frac{1}{N}\sum_{i=1}^{N} x_{i,\mathrm{measured}}; \sqrt{\frac{1}{N}\sum_{i=1}^{N} x_{i,\mathrm{measured}}^2}\right)}$$
$$E_{rms}(x) = \sqrt{\frac{1}{N}\sum_{i=1}^{N}\left(x_{i,\mathrm{modelled}} - x_{i,\mathrm{measured}}\right)^2} \tag{7}$$

Although not used to define model skill in the calibration phase, the absolute and relative bias are used to identify structural over- or underestimation of model variables:

$$\mathrm{bias}(x) = \frac{1}{N}\sum_{i=1}^{N}\left(x_{i,\mathrm{modelled}} - x_{i,\mathrm{measured}}\right)$$
$$\text{rel. bias}(x) = \frac{1}{N}\sum_{i=1}^{N}\left(\frac{x_{i,\mathrm{modelled}} - x_{i,\mathrm{measured}}}{x_{i,\mathrm{measured}}}\right) \tag{8}$$

5.1 *Calibration step 1: wave-related bed friction*

In the first step, one tide with low wave energy (small surf zone, large shoaling zone) was used to calibrate the wave-related bed friction parameter f_w, using only HF wave height data measured outside the surf zone (excluding the seaward-most PT, which as a boundary forcing point was removed from the analysis). XBeach model default values for γ (0.55) and c_f (0.003) were used in all simulations in calibration step 1. Since these parameters only directly affect the HF wave height inside the surf zone (γ) and LF wave heights (c_f), these default values have very little influence on the HF data outside the surf zone used to calibrate f_w.

An automatic optimization routine was used to identify the best value of f_w based on an initial range of 0.00 – 0.80. The results of this optimization are shown graphically in Figure 2, and calibrated f_w values for each site are given in Table 2.

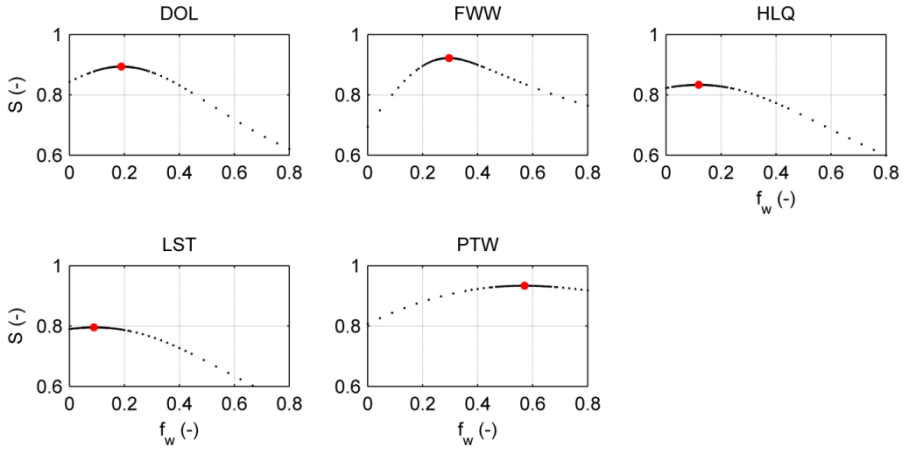

Figure 2. Results of calibration step 1, wave-related friction factor versus model skill at five sites. The red dots indicate the optimal value.

5.2 *Calibration step 2: wave breaking and current-related bed friction*

In the second step, one tide with high wave energy (large surf zone, large LF waves) was used to calibrate the wave breaker parameter γ and the current-related (LF wave-related) bed friction parameter c_f, using LF wave height data (excluding the seaward-most PT, which as a boundary forcing point was removed from the analysis) and only HF wave height data measured inside the surf zone. The value of f_w was set to that found in step 1.

An automatic optimization routine was used to simultaneously identify the best values of γ and c_f, based on an initial range of 0.25 – 0.85 and 0.00 – 0.30, respectively. The results of this optimization are shown graphically in Figure 3, and calibrated of γ and c_f values for each site are given in Table 2. The low value of c_f at PTW is surprising, and is discussed in greater detail in Section 7. It should furthermore be noted that the calibrated values of γ are lower than those typically applied for sandy coasts (e.g., Roelvink, 1993). This differs from settings found by Poate, et al., (submitted) for a simplified stationary wave energy balance model, and merits further investigation. This investigation is however beyond the scope of the current study.

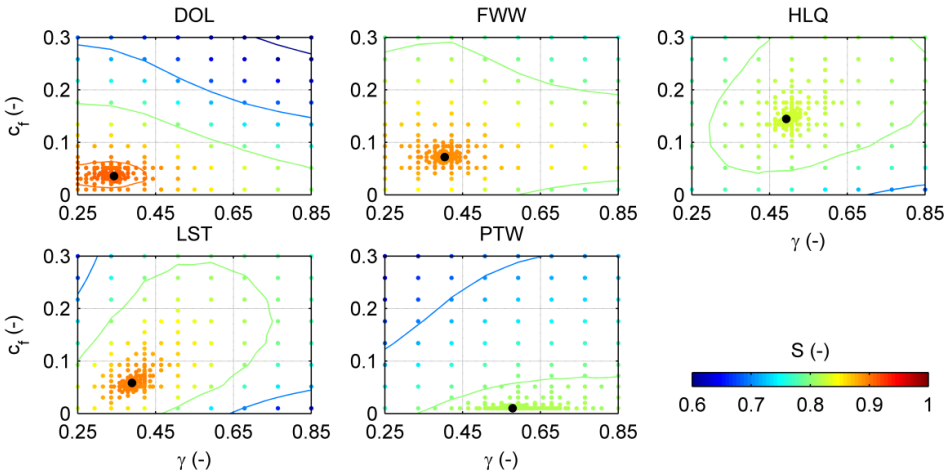

Figure 3. Results of calibration step 2, wave breaker parameter and current-related friction factor versus model skill at five sites. The black dots indicate the optimal value..

Table 2. Calibrated model settings.

Site	f_w (-)	γ (-)	c_f (-)
DOL	0.189	0. 343	0. 036
FWW	0. 296	0. 404	0. 072
HLQ	0. 119	0. 493	0. 145
LST	0. 089	0. 389	0. 058
PTW	0. 570	0. 579	0.010

6. Model validation

The XBeach models of the five rocky shore platforms were validated using the calibrated model settings of Table 2 and model simulations of the 10 – 13 tides that were not used during model calibration. Model predictions of HF and LF wave height at all PTs (excluding the seaward-most PT, which as a boundary forcing point was removed from the analysis) were compared to measurements for every 20-minute data burst described in Section 3. An example of measured and modelled wave heights for one 20-minute burst is given in Figure 4, which shows good correspondence between measured and modelled HF wave dissipation and, in general, LF wave growth (through shoaling and non-linear energy transfer) at all five sites.

Measured wave heights versus modelled predictions for all 20-minute bursts are shown in Figure 5. The figure shows good correspondence between measured and modelled HF wave heights, with little scatter or bias. The model also shows reasonably good correspondence with measured LF wave heights at DOL, FWW (with exception of some low LF-energy conditions) and LST, and somewhat more scatter at HLQ and PTW.

In quantitative terms, the model skill statistics listed in Table 3 indicate that the model can well represent observed HF wave heights, with low RMS errors (HF: Erms 0.06 – 0.08 m, SI ≤ 0.11), slight bias (underestimation bias 0.01 – 0.05 m; relative bias ≤ 7%), and high correlation (ρ ≥ 0.95). LF wave heights are predicted with approximately equal absolute error compared to HF waves (E_{rms} 0.02 – 0.06 m), but greater relative error due to lower measured LF wave heights (SI 0.16 – 0.27). As visible in Figure 5, the greatest relative error in the prediction of LF wave height is at HLQ and PTW. Overall, the results of the validation simulations show that the model, once adequately calibrated, is capable of describing the transformation of HF and LF waves across the five rock platforms well.

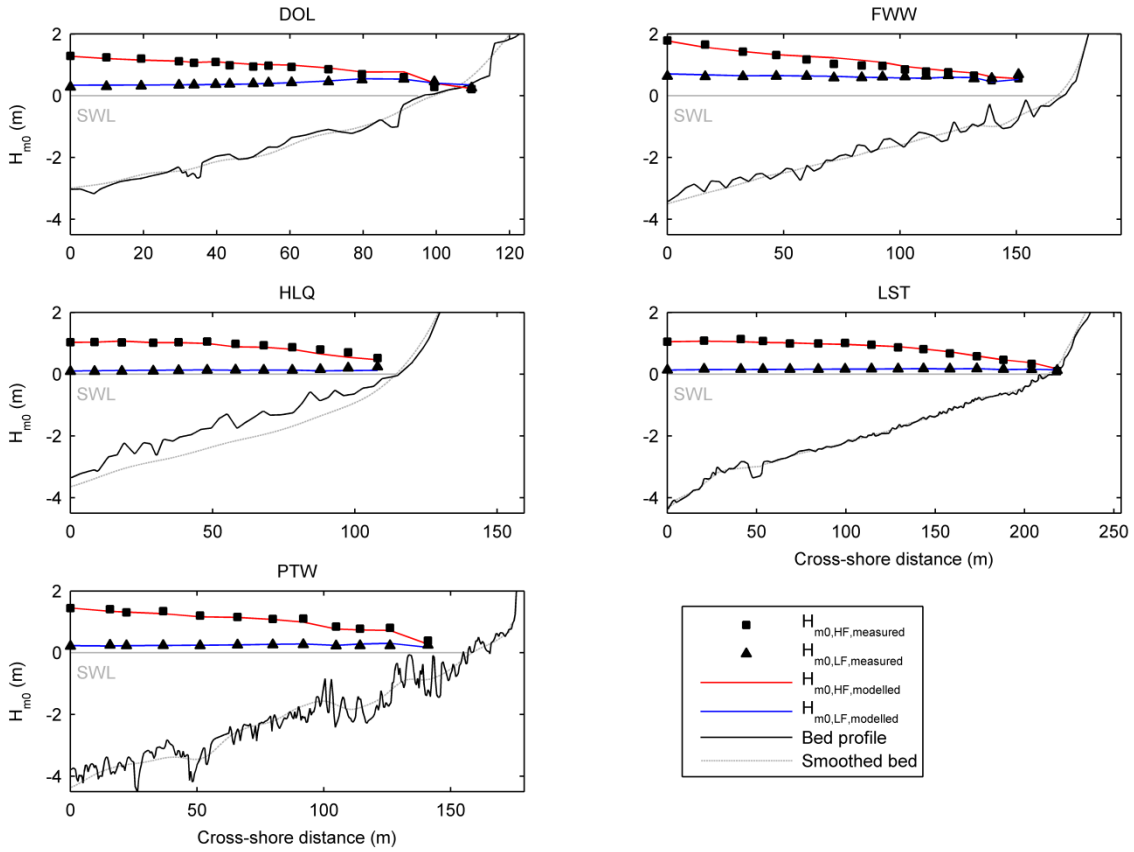

Figure 4. Examples of modelled (lines) and measured (symbols) HF and LF wave transformation across the rock platforms computed over one 20-minute period. All examples taken at mid high-tide, with most PTs submerged. Note that the bed elevation is shown relative to the 20-minute average SWL.

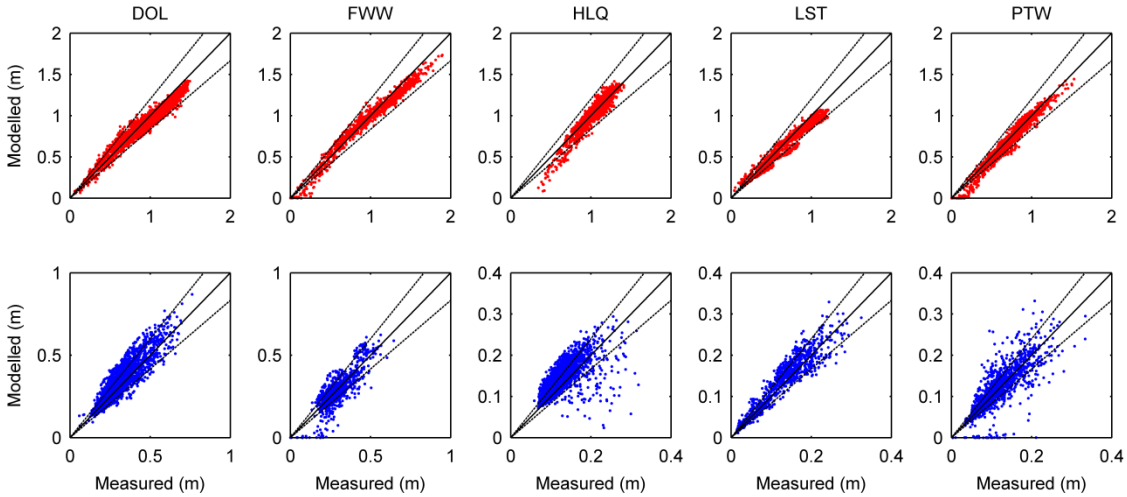

Figure 5. Scatter plots of measured versus modelled HF (top panels; red) and LF (bottom panels; blue) significant wave height. The solid lines indicate a 1:1 relation, the dashed lines indicate a 20% deviation from 1:1.

Table 3. Model validation statistics.

	Site	E_{rms} (m)	SI (-)	Bias (m)	Rel. bias (-)	ρ
High-frequency wave height	DOL	0.08	0.08	-0.04	-0.03	0.98
	FWW	0.08	0.08	-0.02	-0.04	0.98
	HLQ	0.07	0.07	-0.01	-0.02	0.95
	LST	0.08	0.11	-0.05	-0.06	0.98
	PTW	0.06	0.08	-0.03	-0.07	0.98
Low-frequency wave height	DOL	0.06	0.17	0.03	0.09	0.89
	FWW	0.06	0.19	-0.01	-0.03	0.83
	HLQ	0.04	0.27	0.02	0.16	0.63
	LST	0.02	0.16	0.01	0.08	0.95
	PTW	0.03	0.26	0.00	0.02	0.80

7. Platform roughness and model friction settings

For the XBeach model to be applied on other rock platform sites, where fewer or no wave measurements exist with which to calibrate the model, an estimate of the bed friction parameters f_w and c_f is required. Unfortunately, the calibrated values of the friction parameters (Table 2) show a large spread (f_w: 0. 089 – 0.570; c_f: 0.010 – 0.145), and therefore by themselves do not constitute a useful guideline.

To better understand the variation in value of bed roughness parameters, their calibrated values are shown for each site as a function of platform rugosity in Figure 6 (black squares). The figure shows a clear relation between rugosity and the HF wave-related friction parameter, with increasing values of f_w for increasing k_R. Interestingly, the figure does not show a clear increase in the LF wave-related friction factor c_f for increasing k_R, with HLQ and PTW clearly not falling in a general trend.

It is thought that particularly the apparently low value of c_f at PTW is due to the explicit inclusion of bed roughness elements in the model bathymetry (cf. Figure 4, solid black line). Variations in bed level can lead to LF wave energy losses in the solution of the non-linear shallow water equations through contraction and expansion (turbulent viscosity) and LF wave breaking, thereby explicitly resolving a large part of the processes that are otherwise captured in the bed friction parameterization.

To analyze this further, new XBeach models were set up for all five platforms in which the bed elevation is derived from a 5 x 5 m-average of the terrestrial laser scanner DEM (Figure 4, dashed grey), thereby removing the majority of the small-scale bed level variations experienced by the model. The models were subsequently recalibrated using the same data and routines as described in Section 5.

The resulting optimized model parameters are given in Table 4. The table shows similar values for f_w as

found using the original bed elevation in Table 2, with only PTW showing any substantial variation. This indicates that the HF wave action balance equations are not highly sensitive to small-scale bed elevation variations. The calibrated values of c_f vary more substantially between simulations on the original bed and the smoothed bed, particularly for the rougher sites HLQ, FWW and PTW.

The calibrated bed friction parameters for the smoothed bed models are shown as a function of platform rugosity in Figure 6 (grey circles). The results confirm the relation found between k_R and f_w in the original model simulations. However, in the case of the LF wave-related bed friction parameter, the results show a more consistent trend of increasing values of c_f with increasing k_R.

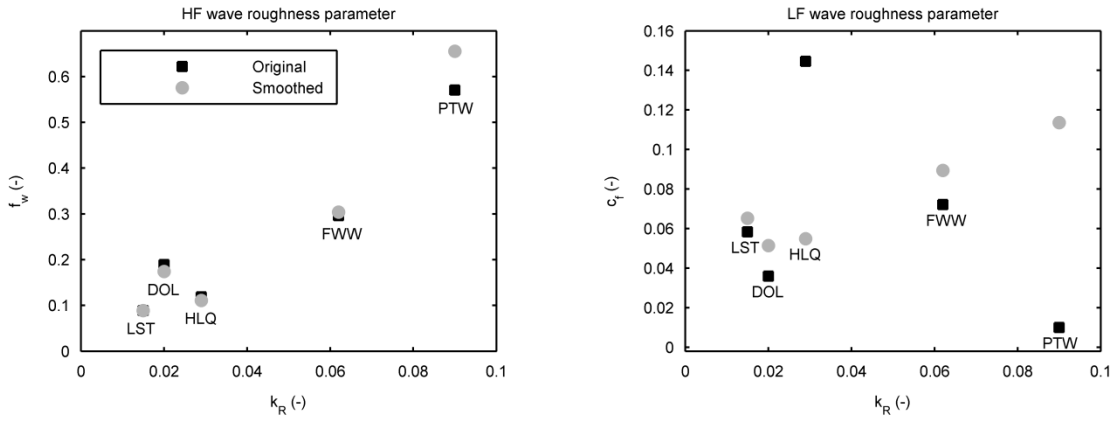

Figure 6. Platform rugosity versus the HF wave-related friction factor (left panel) and the LF wave-related friction factor (right panel). Black squares indicate values found in the calibration stage, grey circles indicate values found using a smoothed bed profile.

Table 4. Calibrated model settings for smoothed beds.

Site	f_w (-)	γ (-)	c_f (-)
DOL	0.174	0. 350	0. 051
FWW	0. 304	0. 389	0. 089
HLQ	0. 111	0. 346	0. 055
LST	0. 089	0. 389	0. 065
PTW	0. 656	0. 593	0.114

As was the case for the original models of the rock platforms, the calibrated bed friction settings for the models with smoothed profiles were validated using the same data and methods described in Section 6. Interestingly, the results presented in Table 5 show that model skill for both HF and LF waves is not substantially increased or decreased when using the smoothed bed profiles (in combination with their associated calibration settings) relative to the original simulations. The slight exceptions are FWW (slight improvement in LF wave heights), HLQ (increased scatter and bias in the LF wave height) and PTW (improvement in scatter and correlation of LF wave height). The results indicate that given sufficient wave data with which to calibrate, accurate results may achieved even if less detailed bed elevation data are available. Conversely, if no wave data are available with which to calibrate bed roughness settings, smoothing the measured platform topography and applying similar bed friction parameter values as those shown in Figure 6 (grey circles), may improve predictions of LF waves relative to a simulation on an unsmoothed bathymetry and unknown settings for the bed roughness parameters.

Table 5. Model validation statistics for smoothed bed models. Differences greater than 2 cm or 2 percentage points relative to the scores in Table 3 are highlighted green (greater accuracy with smoothed bed) or red (lesser accuracy).

	Site	E_{rms} (m)	SI (-)	Bias (m)	Rel. bias (-)	ρ
High-frequency wave height	DOL	0.08	0.09	-0.04	-0.03	0.98
	FWW	0.08	0.07	-0.01	**0.03**	0.99
	HLQ	0.06	0.06	-0.01	-0.01	0.97
	LST	0.09	0.11	-0.06	-0.06	0.98
	PTW	0.06	0.08	**-0.00**	**0.02**	0.98
Low-frequency wave height	DOL	0.06	0.17	0.02	0.07	0.88
	FWW	0.05	**0.16**	-0.00	**-0.00**	**0.86**
	HLQ	0.05	**0.33**	0.04	**0.30**	**0.78**
	LST	0.02	0.16	0.01	0.07	0.95
	PTW	0.02	**0.17**	-0.01	**-0.03**	**0.90**

To highlight however the importance of including (parameterized) bed friction in the modelling of wave transformation across rock platforms, sensitivity simulations were carried out for the smoothest (LST) and roughest (PTW) platform in which the model bed friction parameters were turned on (using calibrated values), or off. Simulations were run for the two tides used in the calibration phase (Section 5), and comprise both mild and energetic wave conditions. All simulations were run using the smoothed bed elevation described in Section 7 to ensure that the effect if switching off the parametric bed friction term was not masked by LF wave energy losses due to the model bed elevation variations, as seen at PTW in Figure 6.

The results of the sensitivity simulations are shown in Figure 7 alongside the observed HF and LF wave height. The figure shows that with the exception of HF wave energy on the smoothest platform (LST), HF and LF wave heights are greatly reduced in the model by the presence of (parameterized) bed friction. It is important to note in particular that the LF wave height is strongly affected by dissipation due to bed friction (through the c_f parameter). This is the case even at LST, which is relatively smooth and where the HF wave transformation is not strongly affected by bed friction. Calibration of bed friction based on HF wave heights alone is therefore unlikely to produce accurate predictions of LF wave transformation across the platform.

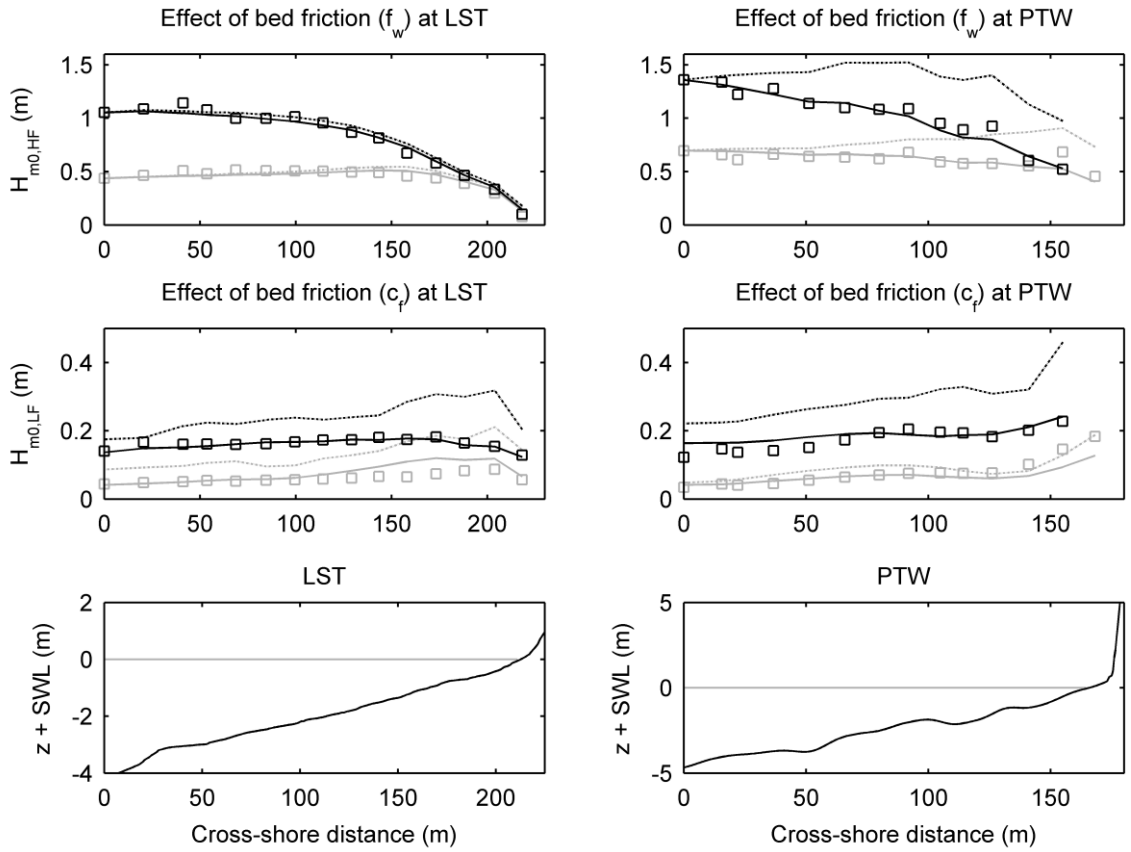

Figure 7. Model predictions of HF (top row) and LF (center row) wave height for two wave conditions (energetic: black lines; mild: grey lines) and including (solid) and excluding (dashed) bed friction, at LST (left column) and PTW (right column). Squares indicate observed values. The smoothed bed elevation applied in the models is shown relative to SWL in the bottom row.

8. Conclusions

In this work we use the process-based model XBeach to simulate high-frequency (HF; incident-band) and low-frequency (LF; infragravity) wave transformation across rocky shore platforms. The model was calibrated using unique measurements of bed elevation and roughness, and hydrodynamics on five rock platforms under mild to energetic wave conditions collected during the WASP (Waves Across Shore Platforms) project (Poate, et al., 2016; Poate, et al., submitted). Validation of the model using calibrated settings for bed friction and wave breaking show that the model is capable of reproducing HF and LF wave heights across the platform with little scatter (scatter index 0.07 – 0.27) and bias (-0.05 – + 0.02 m). Results of the model calibration indicate a strong relation between optimal HF wave-related bed friction parameter values and platform rugosity, but no clear relation between LF wave-related bed friction parameter values and platform rugosity. Reducing topographic detail (removing small-scale bed elevation variations) and recalibrating model parameters leads to similar model accuracy as for simulations carried out using the detailed topography, and additionally does show a clear relation between LF wave-related bed friction parameter values and platform rugosity. In application on sites with little validation data, an approach using smoothed topography and higher parameterized bed friction based on the platform rugosity may therefore provide more accurate results. Sensitivity studies furthermore show that calibration of the model should be carried out for both HF and LF waves, as even relatively smooth platforms that do not strongly affect HF wave transformation through bed friction were still shown to dissipate significant amounts of LF wave energy through bed friction.

Acknowledgements

This research was funded by EPSRC grant EP/L02523X/1, Waves Across Shore Platforms, awarded to GM and MA. RM would like to acknowledge support given by Deltares through the Strategic Research in the "Hydro- and morphodynamics during extreme events" program (1230002).

References

Beetham, E., and Kench, P.S., 2011. Field observations of infragravity waves and their behaviour on rock shore platforms. *Earth Surface Processes and Landforms*, 36: 1872–1888. doi: 10.1002/esp.2208.

Bird, E., 2000. *Coastal Geomorphology: An Introduction*. Chichester: Wiley.

De Vet, P.L.M., R.T. McCall, J.P. Den Bieman, M.J.F. Stive and M. Van Ormondt, 2015. Modelling dune erosion, overwash and breaching at Fire Island (NY) during Hurricane Sandy. *Proc. Coastal Sediments 2015*.

Dickson, M. E., H. Ogawa, P. S. Kench, and A. Hutchinson, 2013. Sea-cliff retreat and shore platform widening: steady-state equilibrium?, *Earth surface processes and landforms*, 38(9), 1046–1048. Doi: 10.1002/esp.3422.

Dissanayake, P., Brown, J., Karunarathna, H. Modelling storm-induced beach/dune evolution: Sefton coast, Liverpool Bay, UK. *Marine Geology*, 357, 225–242. DOI: 10.1016/j.margeo.2014.07.013

Mansard, E., and Funke, E., 1980. The measurement of incident and reflected spectra using a least squares method. *Proceedings of the 17th International Conference on Coastal Engineering*, ASCE, p. 154–172.

Marshall, R. J. E., and W. J. Stephenson, 2011. The morphodynamics of shore platforms in a micro-tidal setting: Interactions between waves and morphology, *Marine Geology*, 288(1–4), 18-31.Doi: 10.1016/j.margeo.2011.06.007

Masselink, G., McCall, R., Poate, T., Van Geer, P., 2015. Modelling storm response on gravel beaches using XBeach-G. *Proceedings of the Institution of Civil Engineers-Maritime Engineering*, vol. 167, no. 4, pp. 173–191.

McCall, R. T., Van Thiel de Vries, J. S. M., Plant, N. G., Van Dongeren, A. R., Roelvink, J. A., Thompson, D. M., and Reniers, A. J. H. M., 2010. Two-dimensional time dependent hurricane overwash and erosion modeling at Santa Rosa Island. *Coastal Engineering*, 57(7), 668-683.

McCall, R., Masselink, G., Poate, T, Roelvink, J., Almeida, L., 2015. Modelling the morphodynamics of gravel beaches during storms with XBeach-G. *Coastal Engineering*, 103, 52–66

Nielsen, P., 1989. Analysis of Natural Waves by Local Approximations. *Journal of Waterway, Port, Coastal, and Ocean Engineering*, 115(3): 384-396.Doi: 10.1061/(ASCE)0733-950X(1989)115:3(384).

Ogawa, H., Dickson, M. & Kench, P., 2011. Wave transformation on a sub-horizontal shore platform, Tatpouri, North Island, New Zealand. Continental Shelf Research, 31(14), p. 1409–1419.

Ogawa, H., Dickson, M. E., & Kench, P. S. (2015). Hydrodynamic constraints and storm wave characteristics on a sub-horizontal shore platform. *Earth Surface Processes and Landforms*, 40(1), 65-77. Doi:10.1002/esp.3619.

Poate, T., Masselink, G., Austin, M., Dickson, M. and Kench, P., 2016. Observation of Wave Transformation on Macro-tidal Rocky Platforms. *Journal of Coastal Research*, 75(sp1), pp.602-606.

Poate, T., Masselink, G., Austin, M., Dickson, M., and McCall, R, *submitted*. The role of roughness in wave transformation across sloping rock shore platforms. Submitted to *Journal of Geophysical Research: Earth Surface*.

Quataert, E., C. Storlazzi, A. van Rooijen, O. Cheriton, and A. van Dongeren, 2015. The influence of coral reefs and climate change on wave-driven flooding of tropical coastlines, *Geophys. Res. Lett*., 42, 6407–6415, doi:10.1002/2015GL064861.

Roelvink, J., 1993. Dissipation in random wave group incident on a beach. *Coastal Engineering*, 19, 127–150.

Roelvink, D., Reniers, A., Van Dongeren, A., Van Thiel de Vries, J., McCall, R. and Lescinski, J., 2009. Modelling storm impacts on beaches, dunes and barrier islands, *Coastal Engineering*, 56(11), 1133–1152.

Smallegan, S.M., J. L. Irish, J. P. den Bieman, and A. R. van Dongeren, 2015. Numerical investigation of developed and undeveloped barrier island response to Hurricane Sandy. *Proc. Coastal Sediments 2015*.

Sunamura, T., 1992. *Geomorphology of Rocky Coasts*. Chichester: Wiley.

Trenhaile, A. (1983). The Width of Shore Platforms; A Theoretical Approach. *Geografiska Annaler. Series A, Physical Geography*, 65(1/2), 147-158. doi:10.2307/520728

Trenhaile, A., 1987. *The geomorphology of rock coasts*. Oxford: Oxford University Press.

Van Dongeren, A.R., R. Lowe, A. Pomeroy, M.T. Duong, J.A. Roelvink, G. Symonds and R. Ranasinghe, 2012. Numerical modeling of low-frequency wave dynamics over a fringing coral reef. *Coastal Engineering*, doi: 10.1016/j.coastaleng.2012.11.004